frontiers | Frontiers in Earth Science

TYPE Original Research
PUBLISHED 30 August 2022
DOI 10.3389/feart.2022.971031

OPEN ACCESS

EDITED BY
Qingtao Meng,
Jilin University, China

REVIEWED BY
Yu Song,
China University of Geosciences
Wuhan, China
Kun Zhang,
Northeast Normal University, China

*CORRESPONDENCE
Zetang Wang,
wangzetang@cumt.edu.cn
Wenli Zhang,
649069716@qq.com

SPECIALTY SECTION
This article was submitted to Geochemistry,
a section of the journal
Frontiers in Earth Science

RECEIVED 16 June 2022
ACCEPTED 08 August 2022
PUBLISHED 30 August 2022

CITATION
Dong Z, Wang Z, Zhang W, Zhao F, Du Y, Zhu Y, Fu X and Wang C (2022), Dynamic sulfur and carbon cycles related to microbial sulfate reduction and volcanic activity during the Hirnantian glaciation in the Upper Yangtze Basin, South China.
Front. Earth Sci. 10:971031.
doi: 10.3389/feart.2022.971031

Dynamic sulfur and carbon cycles related to microbial sulfate reduction and volcanic activity during the Hirnantian glaciation in the Upper Yangtze Basin, South China

Zaitian Dong[1], Zetang Wang[1]*, Wenli Zhang[2]*, Fei Zhao[3], Yunhang Du[4], Yuxuan Zhu[1], Xuehai Fu[1] and Chaoyong Wang[1]

[1]School of Resources and Earth Sciences, China University of Mining and Technology, Xuzhou, Jiangsu, China, [2]School of Management, Xi'an University of Science and Technology, Xi'an, Shaanxi, China, [3]Xuzhou Datun Engineering Consulting Co., Ltd., Xuzhou, Jiangsu, China, [4]Yunnan Vocational Institute of Energy Technology, Qujing, Yunnan, China

Parallel positive excursions of organic carbon ($\delta^{13}C_{org}$) and pyrite sulfur ($\delta^{34}S_{py}$) isotopes occurred globally during the Hirnantian glacial period. However, the reasons for these isotope excursions and their relationship with paleoenvironmental dynamics are not fully understood. This study presents a high-resolution geochemical investigation of the Tianlin section of the Upper Yangtze Basin, South China. The total organic carbon (TOC), iron speciation, trace elements, $\delta^{13}C_{org}$, and $\delta^{34}S_{py}$ were analyzed and compared with published results from the other four sections in the same basin. A negative relationship was observed for the sulfate reduction index (SRI) with TOC and organic carbon accumulation rate. This suggests that the abundance of sedimentary organic matter was not the main factor inhibiting microbial sulfate reduction (MSR). The significant positive correlations of SRI with pyrite and $\delta^{34}S_{py}$ showed that MSR promoted the formation of pyrite and that the availability of sulfate was the main limiting factor for the $\delta^{34}S_{py}$ change. The negative excursions of $\delta^{13}C_{org}$ and $\delta^{34}S_{py}$ during the pre-glacial and post-glacial periods were coupled with dense segments of bentonite, indicating that volcanism was the main driving force for the negative excursions of C and S isotopes. Moreover, the sulfate input of rivers, restored at the post-glacial period, was the main reason for the continued negative excursion of S isotopes. Our results emphasize the key role of MSR and volcanic activity in C and S isotope excursions and their corresponding environmental changes in semi-restricted basins during the Hirnantian glaciation.

KEYWORDS

sulfur isotopes, carbon isotope, bentonite, sulfate reduction index, Upper Yangtze Basin, Hirnantian

1 Introduction

The Hirnantian Stage (Late Ordovician to Early Silurian, O-S, 445.6–443.7 Ma), was one of the three period in Earth's history with continental glaciers distributed globally (Tumer et al., 2005). With the expansion and dissipation of glaciation, this period also witnessed the first Paleozoic biotic extinction and recovery (Sutcliffe et al., 2000; Sheehan, 2001). At this stage, substantial evidence regarding significant changes in climate and ice cover formation has been found; these changes include the positive excursion of the carbon isotope ($\delta^{13}C$); sea-level fall; the emergence of glacial sedimentary cycles in the Katian Stage; the deposition of carbonate rocks containing flint and phosphate; and an increased global marine $\delta^{18}O$ value (Hambrey, 1985; Kump and Arthur, 1999; Pope and Steffen, 2003; Trotter et al., 2008; Kiipli et al., 2010; Munnecke et al., 2010; Finnegan et al., 2011; Elrick et al., 2013; Yang et al., 2021). Because carbon and sulfur isotopes are closely tied to environmental change and biological innovation, disturbances in these isotopes, as they relate to the complex changes that characterized the Hirnantian Stage, have been studied extensively (Brenchley et al., 2003; Jones and Fike, 2013; Wang et al., 2021a; Zhang et al., 2021a; Li Y et al., 2021).

Numerous studies have highlighted positive excursions in both organic ($\delta^{13}C_{org}$) and carbonate carbon ($\delta^{13}C_{carb}$) during the Hirnantian Stage (e.g., Brenchley et al., 2003; Fan et al., 2009; Zhang et al., 2009; Jones and Fike, 2013). This phenomenon is often explained via two mainstream views. According to the first explanation, before Hirnantian glaciation, the burial of large amounts of organic carbon (i.e., due to high productivity) resulted in the positive deviation of carbon isotope (Qing and Veizer, 1994; Brenchley et al., 2003). The extensive burial of organic carbon that characterizes this period is thought to have also caused a significant decrease in the atmospheric CO_2, culminating in glaciation (Gibbs et al., 1997; Herrmann et al., 2004; Lv et al., 2022). The other explanation is centered on the idea that the input of terrigenous debris (i.e., via carbonate weathering) rich in carbon isotopes, during the glacial periods, promoted the increase of $\delta^{13}C$ in sediments (Kump and Arthur, 1999 (Jones et al., 2011). Additionally, synchronized positive excursions of pyrite sulfur isotopes ($\delta^{34}S_{py}$) have also been observed in the Hirnantian Stage (Yan et al., 2009a; Zhang et al., 2009; Hammarlund et al., 2012). Interpretations of the positive excursions of $\delta^{34}S_{py}$ can be summarized by two mechanisms. First, the burial mechanism points to the possibility that strong microbial sulfate reduction (MSR), under anoxic conditions, resulted in the consumption of sulfate in the water column. The pyrite generated during this process was then buried in large quantities, resulting in a gradual increase in $\delta^{34}S_{py}$ (Zhang et al., 2009; Gill et al., 2011). The other mechanism suggests that the input of Hirnantian oxygen-containing water forced the chemocline into the sediments, limiting the supply of sulfate in the pore water, and then generating ^{34}S-rich pyrite (Yan et al., 2009a; Jones and Fike, 2013). It is apparent that explanations behind the changes in the carbon and sulfur cycles in the Hirnantian Stage are complex, and that more information is needed to comprehensively characterize their relationship.

Data from different profiles have confirmed the occurrence of carbon and sulfur disturbances in the Upper Yangtze Basin during the O-S period, and the effects of the resultant environmental changes. These data also brought forth insights tried to sulfate availability and volcanic activity during this period (Yan et al., 2009b; Zhang et al., 2009; Gorjan et al., 2012; Li et al., 2017a; Li et al., 2019; Li N et al., 2021; Xi et al., 2021). However, a fine-scale study on the effect of MSR on carbon and sulfur cycles has not been conducted to data, and the dynamic mechanism of $\delta^{13}C_{org}$ and $\delta^{34}S_{py}$ negative excursions and their long-term maintenance after a glacial period have not been explained clearly.

In this study, detailed analyses of $\delta^{13}C_{org}$ and $\delta^{34}S_{py}$ were conducted to determine their prevalence during the O-S period. Combined with iron speciation and trace element analysis, mechanisms driving $\delta^{13}C_{org}$ and $\delta^{34}S_{py}$ changes were discussed and analyzed through the lens of MSR and volcanic activity, providing new insights into carbon and sulfur cycles during the Hirnantian Stage.

2 Geological background

The Upper Yangtze Basin, located in the central part of the Yangtze Plate, was dominated by carbonate deposits in the Early Ordovician and covered by vast epeiric seas (Figure 1A). In the Late Ordovician, influenced by the Kwangsian Orogeny, the Yangtze Plate was subjected to the subduction and compression of the Cathaysian plate in the southeast, and gradually surrounded by several paleo-continents and uplifts (Zhou et al., 2015). At this time, the Qianzhong uplift in the south was connected to the Xuefeng uplift, and the Kangdian paleocontinent and Chuanzhong uplift in the west continued to expand, inducing a low-energy, compensational stacking of sediment within the plate (Figure 1B). Petrographically, carbonate rocks have been replaced by terrigenous clastic deposits–from the Baota Formation and Linxiang Formation limestone to the O-S Wufeng-Longmaxi (WF-LMX) Formation black shale deposits (Chen et al., 2004).

The Tianlin section (27°55′15″N, 105°36′45″E) is in the southern sedimentary center of the Upper Yangtze Basin (Figure 1B). This section reveals complete strata containing the entire Ordovician–Silurian boundary. From bottom to top, it is composed of carbonaceous and siliceous black shale from the

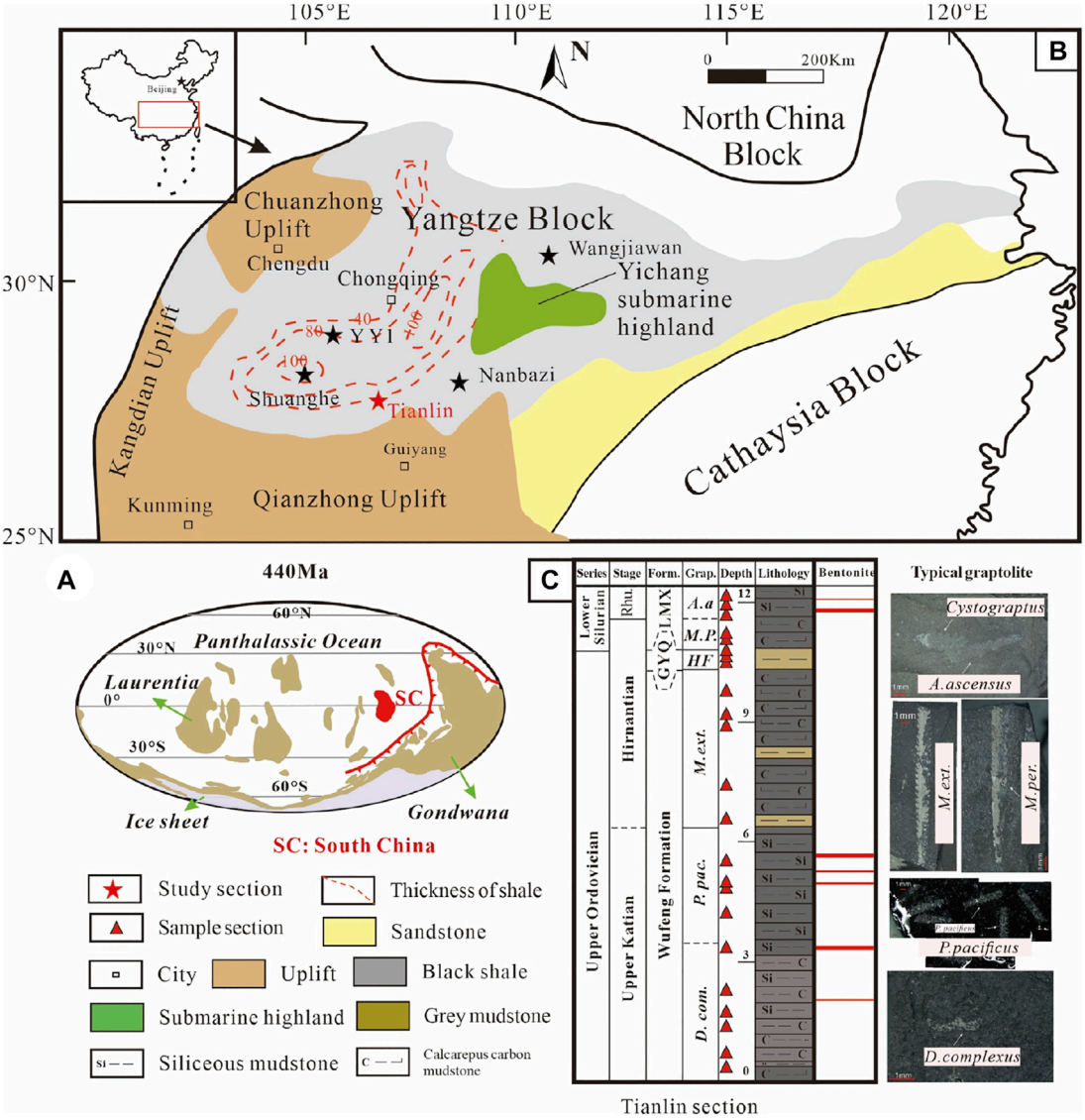

FIGURE 1
Paleogeographic context and geological setting of the Tianlin section. **(A)** Global paleogeography for the Late Ordovician (~445 Ma) (Zhou et al., 2015). **(B)** Paleogeography of the Upper Yangtze Basin from the Late Ordovician to Early Silurian (modified from Liu et al., 2016) **(C)** Biostratigraphy and bentonite distribution for the Tianlin section (graptolite biozones based on Chen et al. (2004). GYQ, Guanyinqiao Formation; *HF*, *Hirnantia Fauna*).

WF Formation of the Katian stage, argillaceous limestone from the Guanyinqiao (GYQ) Formation of the Hirnantian Stage, and black silty shale from the LMX Formation of the Rhuddanian Stage (Figure 1C). The graptolite biostratigraphy of the Yangtze Basin is well established (Chen et al., 2000; Chen et al., 2004). In the Tianlin section, five graptolite biozones and their estimated yielding durations have been identified from bottom to top, i.e., *D. complexus* ~ 0.6 Myr, *P. pacificus* ~ 1.86 Myr, *M. extraordinarius* ~ 0.73 Myr, *M. persculptus* ~ 0.6 Myr, and *A. ascensus* ~ 0.43 Myr zones (Chen et al., 2004; Cooper et al., 2012).

3 Samples and methods

3.1 Samples

To circumvent the influence of surface weathering, 23 representative fresh shale samples were collected from the Tianlin section via drilling. A BC-20S portable drilling rig was used for sampling. The diameter of the borehole was 36 mm and the depth was 0.15 m. All samples were ground to ≤200 mesh size using an agate mortar, and then $\delta^{13}C_{org}$, $\delta^{34}S_{py}$, and the major and trace elements were evaluated.

3.2 Methods

First, each powder sample (2 g) was placed in a 5 ml centrifuge tube. Then, 5 ml HCl, with a concentration of 4 mol/L, was added to the tube and then shaken. The powder was allowed to dissolve in the HCl for 12 h; its dissolution was considered complete when there was the formation of bubbles stopped. This step was conducted to remove carbonate from the samples. The treated samples were then repeatedly washed and centrifuged with deionized water until the pH of the supernatant reached 7. Once the pH was neutral, the samples were dried thoroughly. Total organic matter (TOC) and total sulfur (TS) were then determined using the LECO CS-200 carbon-sulfur analyzer. $\delta^{13}C_{org}$ was determined using an isotope ratio mass spectrometer (MAT-253). The organic carbon isotope composition was calibrated using USG ($\delta^{13}C$ = −23.39‰) and UREA ($\delta^{13}C$ = −37.32‰), and the analysis results were uniformly expressed as $\delta^{13}C$ relative to the Vienna Pee Dee Belemnite (VPDB). $\delta^{34}S$ was determined via the chromium reduction method (Canfield and Farquhar, 1986), and the sulfur isotope of the generated sulfide was analyzed using by Thermo Fisher Scientific Delta V Plus mass spectrometer and Costech ECS 4010 elemental analyzer. The sulfur isotope composition was calibrated using IAEA-S1 (−3.0‰), IAEA-S2 (22.65‰), and IAEA-S3 (−32.5‰), and the analysis results were uniformly expressed as $\delta^{34}S$ relative to the Vienna-Canyon Diablo Troilite (V-CDT). The accuracy of carbon and sulfur isotope analyses was 0.2‰. All experimental tests were conducted at the State Key Laboratory of Biogeology and Environmental Geology, China.

Major and trace elements were tested at the Jiangsu Geological and Mineral Resources Design and Research Institute using the Bruker S8 Tiger X-ray fluorescence spectrometer (XRF) and the PE Elan600 standard inductively coupled plasma mass spectrometer (ICP-MS), respectively. The specific steps and standards involved in this step can be found in a previous study (Wang et al., 2021a; Zhang et al., 2021b).

The content of mercury (Hg) was determined using the DMA-80 automatic mercury analyzer at the School of Resources and Earth Sciences, China University of Mining and Technology. Specifically, 100 mg dried shale powder samples were weighed and put into a cracking furnace. Mercury vapor was released under the action of a high temperature catalyst, and the carrier gas was moved into an optical cell for determination at a wavelength of 253.7 nm.

Additionally, we used the organic carbon accumulation rate (OCAR) to evaluate the characters of primary productivity (Schoepfer et al., 2015). The following formula was used OCAR = TOC × LSR × ρ, where ρ = 2.5g/cm^{-3}, represents the density of bulk rock (Shen et al., 2015). LSR is the linear sedimentation rate.

4 Results

All geochemical data, $\delta^{13}C_{org}$, and $\delta^{34}S_{py}$ results of the Tianlin section are presented in Table 1 and Figure 2. The test data for the Shuanghe section, YY1 well, Wangjiawan section and Nanbazi section can be found in previous studies (Yan et al., 2009b, 2012; Liu et al., 2016; Li et al., 2017b; Li Y et al., 2021).

4.1 TOC content and organic carbon isotope

Results of the TOC content for the Tianlin section ranged from 0.59 to 7.17% (average=3.01%). For the WF Formation (including the Late Katian stage and Early Hirnantian Stage), the TOC content ranged from 0.79 to 4.99% (average = 2.85%). In the GYQ Formation, it ranged from 0.59 to 1.54% (average = 1.18%). Comparatively, for the LMX Formation, the TOC value increased sharply from 3.11 to 7.17% (average = 4.60%) (Table 1 and Figure 2A). The distribution of OCAR showed a trend similar to that of TOC (Figure 2A). From the Late Katian Stage to Early Rhuddanian Stage, OCAR first decreased and then increased.

Results of the $\delta^{13}C_{org}$ for the Tianlin section ranged from −30.8‰ to −29.6‰ (average = −30.3‰). From the WF Formation to GYQ Formation, and then to the LMX Formation, the $\delta^{13}C_{org}$ values first increased from −30.41‰ to −29.73‰, and then decreased to −30.48‰ (Table 1 and Figure 2E). Although the values of $\delta^{13}C_{org}$ were generally low in organic-rich layers and high in organic-poor layers, there was no significant correlation between TOC and $\delta^{13}C_{org}$ (Figure 3A), suggesting that the $\delta^{13}C_{org}$ was less affected by the original productivity of OM, and recorded important information about the global carbon reservoir changes during the O-S period (Kump and Arthur, 1999).

4.2 TS content and pyrite sulfur isotope

Results of the TS content for the Tianlin section ranged from 0.03 to 2.16% (average = 1.20%) (Figure 2B). Additionally, there was a significant positive correlation between Fe_{py} and TOC (r = 0.67, $p < 0.01$, n = 23) (Figure 3B), indicating that the abundance of organic matter (OM) could be a factor that controlled the formation of pyrite.

$\delta^{34}S_{py}$ varied across a large range, from −9.60 to 11.7‰ (average = −1.38‰) (Figure 2E). The change in $\delta^{34}S_{py}$ was similar to that in $\delta^{13}C_{org}$, with the highest value observed for the Hirnantian Stage, particularly in the GYQ Formation (11.7‰ for sample TL-18; Table 1 and Figure 3C). Additionally, there was a negative correlation between $\delta^{34}S_{py}$ and Fe_{py} (r = −0.48, $p < 0.05$, Figure 3D), indicating that the availability of sulfate may control pyrite formation (Li et al., 2019).

TABLE 1 Results of the major, trace elements, $\delta^{13}C_{org}$ and $\delta^{34}S_{py}$ in the Tianlin section.

Stage	Formation	Samples	Depth (m)	$\delta^{34}S_{py}$ (‰)	$\delta^{13}C_{org}$ (‰)	Al (%)	Fe_T (%)	SRI	Fe_{HR}/Fe_T	Fe_{py}/Fe_{HR}	Mo (ppm)	U (ppm)	Hg (ppb)
Rhuddanian	Longmaxi	TL-23	12.10	−5.5	−30.6	4.07	3.58	1.16	0.81	0.59	83.1	11.1	71.9
	Formation	TL-22	11.85	−6.4	−30.6	5.43	3.49	1.44	0.76	0.66	105.6	16.5	149.8
		TL-21	11.33	−1.5	−30.3	6.11	2.23	1.42	0.56	0.67	65.3	16.3	210.4
Hirnantian	GYQ	TL-20	10.88	−7.4	−30.5	5.69	3.26	1.51	0.84	0.68	57.5	38.0	171.2
		TL-19	10.45	−4.4	−30.4	5.23	2.09	1.44	0.74	0.57	75.2	35.0	77.9
		TL-18	10.36	11.7	−29.6	7.00	1.78	1.74	0.34	0.31	8.7	5.1	64.3
	Formation	TL-17	10.25	6.8	−29.8	6.64	1.45	1.03	0.19	0.45	19.6	7.3	45.6
		TL-16	10.10	5.9	−29.8	7.64	2.00	1.05	0.21	0.55	17.9	6.4	56.7
	Wufeng	TL-15	9.94	2.3	−30.4	6.58	2.37	1.33	0.37	0.61	71.9	34.9	41.6
	Formation	TL-14	9.28	1.1	−30.5	6.85	2.25	1.33	0.69	0.57	50.4	24.8	45.6
		TL-13	8.95	−0.9	−29.8	3.81	1.37	1.35	0.55	0.63	11.2	4.6	103.2
		TL-12	7.54	−4.2	−30.2	4.15	1.41	1.41	0.64	0.56	12.7	6.6	74.3
		TL-11	6.40	1.1	−30.4	5.09	1.48	1.31	0.71	0.67	6.4	7.9	88.9
Late Katian		TL-10	5.88	−2.9	−30.6	5.83	1.48	1.37	0.69	0.55	15.3	7.6	201.1
		TL-05	5.32	−3.8	−30.5	5.51	2.25	1.51	0.68	0.41	30.1	14.4	147.9
		TL-05	4.83	−5.9	−30.8	4.97	1.6	1.45	0.59	0.66	35.9	17.5	186.4
		TL-05	4.05	1.7	−30.4	4.03	1.57	1.46	0.66	0.64	6.5	9.7	104.3
		TL-05	3.30	−3.1	−30.2	5.11	2.15	1.45	0.56	0.49	13.0	8.1	194.2
		TL-05	2.45	−5.5	−30.6	7.06	3.30	1.48	0.51	0.66	25.6	13.3	142.3
		TL-04	1.90	1.8	−30.5	6.00	2.64	1.55	0.39	0.58	5.5	4.0	77.8
		TL-03	1.35	2.4	−30.3	8.17	2.72	1.58	0.64	0.67	4.4	2.9	66.5
		TL-02	0.84	−9.6	−30.8	4.64	1.51	1.33	0.31	0.54	0.9	1.8	89.5
		TL-01	0.30	−5.4	−30.2	6.63	3.19	1.56	0.34	0.43	1.3	3.2	91.4

4.3 Major and trace element contents

Iron speciation and its proportional relationship have been widely used to determine the redox conditions of paleowater columns (Poulton and Canfield, 2011; Li et al., 2015). The Fe_T values of all samples were >0.5% (ranging from 1.37 to 3.58%, average = 2.22%; Table 1 and Figure 2B). Fe_{HR}/Fe_T and Fe_{py}/Fe_{HR} showed similar trends from the WF Formation to GYQ Formation, and then to the LMX Formation; these trends are characterized by an initial decrease followed by an increased (Figure 2C). Particularly, the Fe_{HR}/Fe_T and Fe_{py}/Fe_{HR} values of the GYQ Formation samples were the lowest, at 0.25 and 0.44 (average values), respectively (Table 1).

Results of the Al content for the Tianlin section ranged from 3.81 to 8.17% (average = 5.75%) (Table 1). Hg concentrations in the samples ranged from 41.6 to 210.4 ppb (average = 108.8 ppb) (Table 1). The highest average content was 166.8 ppb, at the late Katian Stage, whereas the lowest value was 55.5 ppb, at the Hirnantian Stage. The Mo_{EF} and U_{EF} contents showed similar trends to that of iron speciation (Figure 2D), which first decreased and then increased. In this study, U_{EF} and Mo_{EF} were calculated using the following equation $X_{EF} = (X/Al)\ sample/(X/Al)_{PAAS}$, where PAAS represents the values of corresponding elements for post Archean average shale (Taylor and McClcnnan, 1985). Additionally, the Mo_{EF} and U_{EF} values of the GYQ Formation samples reached lowest average values of 18.33 and 8.20, respectively (Table 1).

5 Discussion

The variation in $\delta^{13}C_{org}$ and $\delta^{34}S_{py}$ values in the Tianlin section of the Yangtze Basin from the late Katian to early Rhuddanian stages was consistent with that of the other four sections in the same basin (Figure 4); additionally, it was also consistent with the data for other basins (e.g., Scotland and Denmark) (Kump and Arthur, 1999; Hammarlund et al., 2012). Both isotopes showed positive excursions during the late Hirnantian Stage (i.e., GYQ Formation), further showing that this is a global phenomenon. To further constrain the evolution of carbon and sulfur during the Hirnantian glaciation period, graptolite biostratigraphy was used to discuss the duration and control mechanism of $\delta^{13}C_{org}$ and $\delta^{34}S_{py}$ excursions.

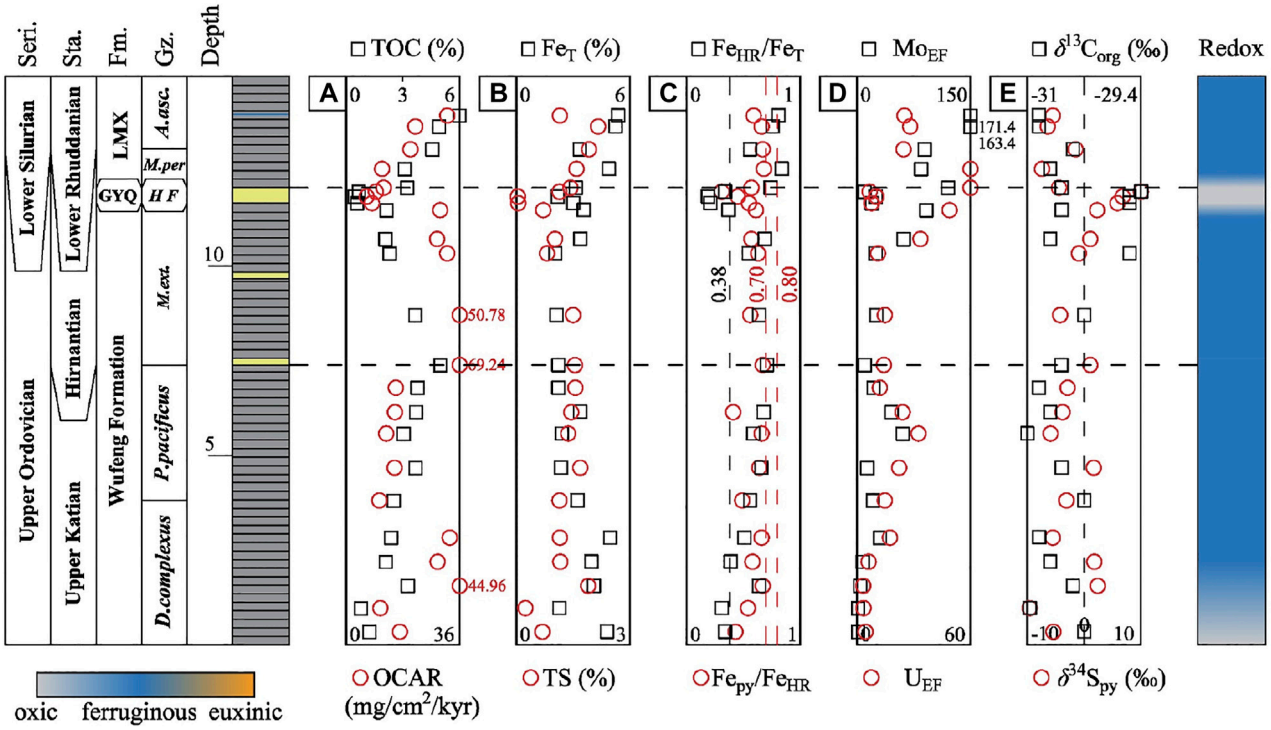

FIGURE 2
Chemo-stratigraphic profiles of **(A)** TOC and OCAR, **(B)** Fe$_T$ and TS, **(C)** Fe$_{HR}$/Fe$_T$ and Fe$_{py}$/Fe$_{HR}$, **(D)** Mo$_{EF}$ and U$_{EF}$, **(E)** $\delta^{13}C_{org}$ and $\delta^{34}S_{py}$, and a redox summary for the Tianlin section. Vertical dotted lines represent the threshold for each proxy.

5.1 Water restriction and redox conditions

5.1.1 Water restriction

The enrichment of sedimentary OM and biogeochemical cycles of elements are controlled by the degree of water restriction (Rowe et al., 2008; Algeo and Rowe, 2012). Geochemical characteristics and the enrichment of Mo and U are often used to determine the degree of water restriction (Algeo and Tribovillard, 2009; Wang et al., 2021a). Specifically, Mo and U show different adsorption rates and degrees of enrichment in restricted and non-restricted water columns under suboxic-to-anoxic conditions, and the covariant relationship between U$_{EF}$ and Mo$_{EF}$ is often used to determine the degree of water restriction (Tribovillard et al., 2012).

In the Tianlin section, from the Late Katian to Early Hirnantian stage (i.e., *M. extraordinarius*), the contents of U and Mo in the samples showed a gradually increase, increasing the value of U$_{EF}$-Mo$_{EF}$ from 0.1×SW to 1×SW (SW, represents sea water; the value of 1×SW is 7.9), but remained less than 1×SW, representing a restricted environment (Tribovillard et al., 2012) (Figure 5A). From the Hirnantian to early Rhuddanian stages, the contents of U and Mo first decreased and then increased, but the value of U$_{EF}$-Mo$_{EF}$ was close to 1×SW, representing a semi-restricted environment (Figure 5A). Combining these results with the YY1 well and Shuanghe section, it is clear that the Upper Yangtze Basin was always in a semi-restricted state during the O-S period (Figure 5B).

5.1.2 Redox conditions

The redox conditions of water not only play an important role in controlling the preservation of sedimentary OM and the formation of black shale, but also restrict the spatial distribution of microorganisms, especially anaerobic ones (Hammarlund et al., 2012; Jones and Fike, 2013; Gomes and Hurtgen, 2015). Iron speciation and its ratios are reliable indicators for determining redox conditions in water columns (Poulton and Canfield, 2011; Li et al., 2015). For samples with Fe$_T$ > 0.5%, Fe$_{HR}$/Fe$_T$ < 0.38 represents oxic conditions; otherwise, its represents anoxic conditions. Additionally, under anoxic conditions, Fe$_{py}$/Fe$_{HR}$ < 0.7–0.8 represents ferruginous conditions, otherwise, it represents euxinic conditions (Poulton and Canfield, 2011). All Fe$_T$ values of the samples were >0.5%, which can be used to determine the redox condition.

From the late Katian to early Hirnantian stages, the value of Fe$_{HR}$/Fe$_T$ ranged from 0.31 to 0.71 (average = 0.56), representing

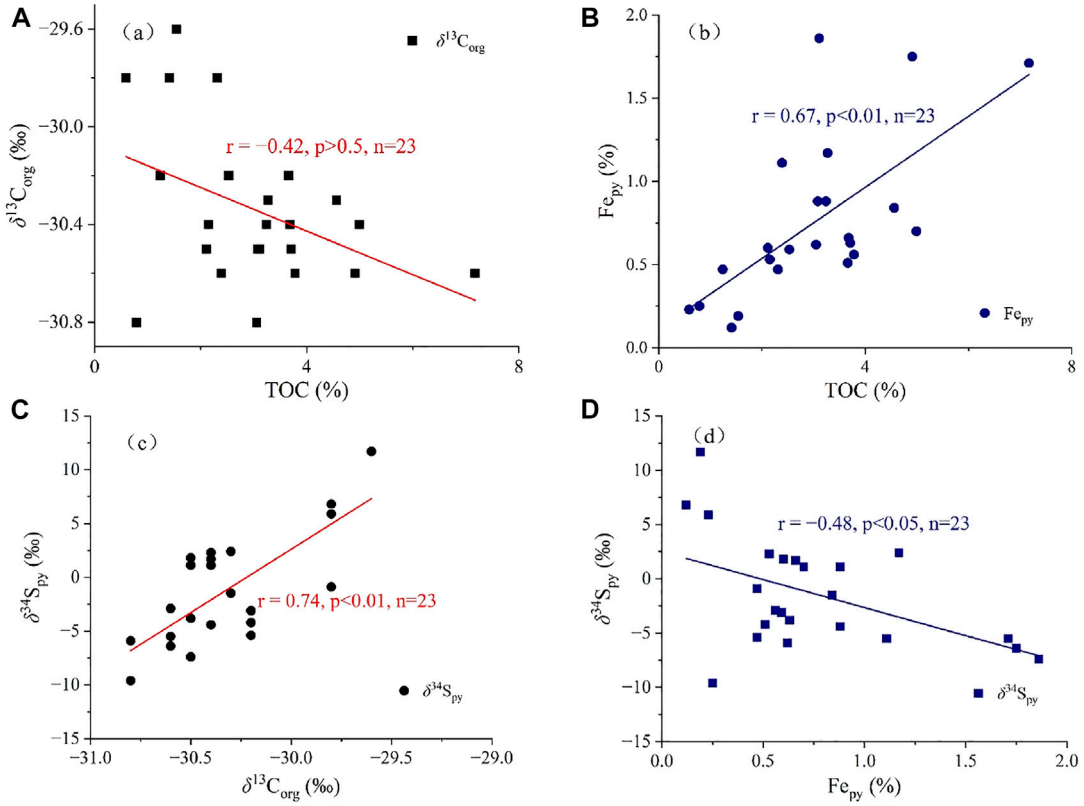

FIGURE 3
Crossplots of TOC vs. **(A)** $\delta^{13}C_{org}$ and **(B)** Fe_{py}, crossplots of **(C)** $\delta^{13}C_{org}$ and **(D)** Fe_{py} vs. $\delta^{34}S_{py}$. All fitting curves are linear.

suboxic to anoxic conditions (Figure 2C). Additionally, the value of Fe_{py}/Fe_{HR} ranged from 0.41 to 0.67 (average = 0.58), suggesting a ferruginous environment. For the GYQ Formation, the value of Fe_{HR}/Fe_T decreased to 0.19, representing oxic conditions. Then, for the early Rhuddanian Stage, the value of Fe_{HR}/Fe_T increased to 0.71, and the Fe_{py}/Fe_{HR} values increased to 0.64 (on average), suggesting that the water conditions returned to being ferruginous conditions (Figure 2). Comparing these data with those of the other three sections, we found that the Upper Yangtze Basin was dominated by anoxic ferruginous conditions before and after the Hirnantian glacial period, and that transient oxic-suboxic conditions occurred in the early late Katian Stage and GYQ Formation period (Figure 6).

Additionally, the degree of water anoxic varied in different sections, especially in the early stage of the Hirnantian glaciation (i.e., *M. extraordinarius*): when other sections were dominated by ferruginous conditions, while, Shuanghe section located in the southwestern sedimentary center of the Upper Yangtze Basin presented euxinic condition (Figure 6). The reasons for the difference in redox conditions are complex, which may be related to the input of terrigenous debris, the effectiveness of sulfate, the changes of sea level and paleoproductivity (Zou et al., 2018; Li et al., 2019; Wang et al., 2021a; Li N et al., 2021; Dong et al., 2022).

5.2 Microbial sulfate reduction effects in marine sediments

In the early diagenesis stage, Fe^{2+} combined with the H_2S generated by the MSR in the water column. This combination formed pyrite, which is an important part of the sulfur cycle (Hurtgen, 2012). This process not only consumes sulfate but it also consumes OM in water, thereby controlling the formation of black shale (Gomes and Hurtgen, 2015). Existing research shows that the abundance of OM, availability of sulfate and the input of active iron jointly controls the strength of MSR (Berner and Raiswell, 1984; Johnston et al., 2005; Raiswell and Canfield, 2012). To effectively evaluate the strength of MSR, the sulfate reduction index (SRI) was introduced (Lallier-Verges et al., 1993). SRI can be calculated using the following equation:

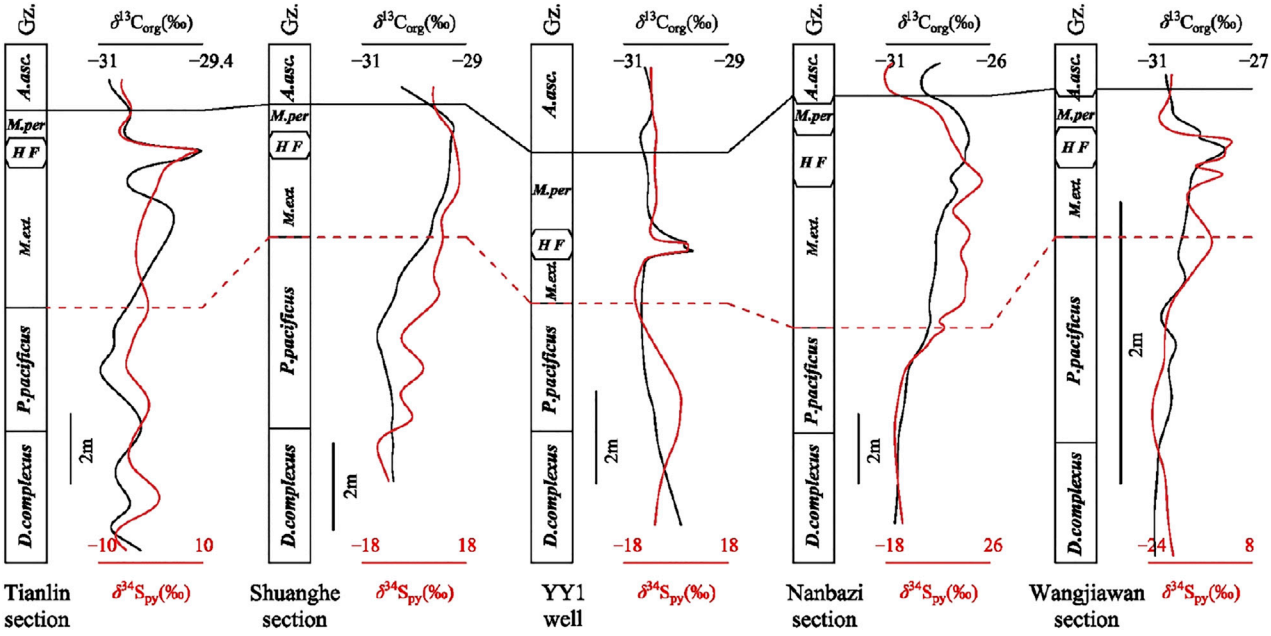

FIGURE 4
Stratigraphic correlation of$\delta^{13}C_{org}$ and $\delta^{34}S_{py}$ sections during the O-S period. Data of the Shuanghe section, YY1 well, Nanbazi section, and Wangjiawan section can be found in previous studies (Yan et al., 2009b, 2012; Liu et al., 2016; Li et al., 2017a; Li N et al., 2021; Li Y et al., 2021).

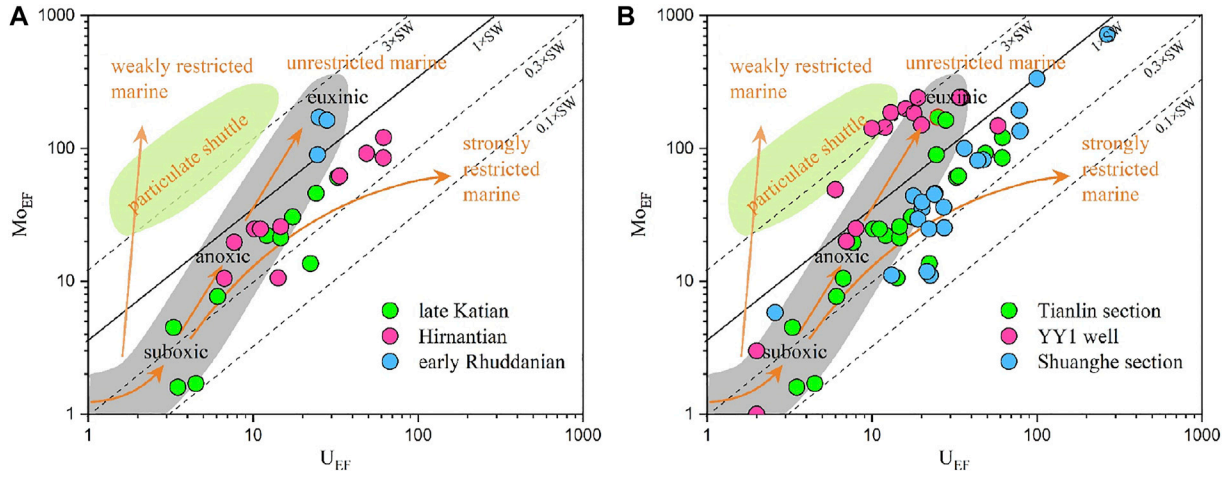

FIGURE 5
Covariant relationship between U_{EF} and Mo_{EF} for the **(A)**Tianlin section and **(B)** Tianlin, YY1 well and Shuanghe sections. The solid line represents the molar concentration ratio of Mo/U in seawater (SW=7.9).

$$SRI = TOC_{OR} / TOC$$

Where TOC_{OR} represents the original carbon content, which was calculated according to previous studies (Berner and Raiswell, 1984; Lallier-Verges et al., 1993; VETO et al., 1994), as $TOC_{OR} = TOC + TOC_{SR}$, where $TOC_{SR} = Total\ sulfar \times 0.75 \times 1.33$.

Thus, the equation for SRI can be rewritten as:

$$SRI = 1 + 0.75 \times 1.33 \times TS/TOC$$

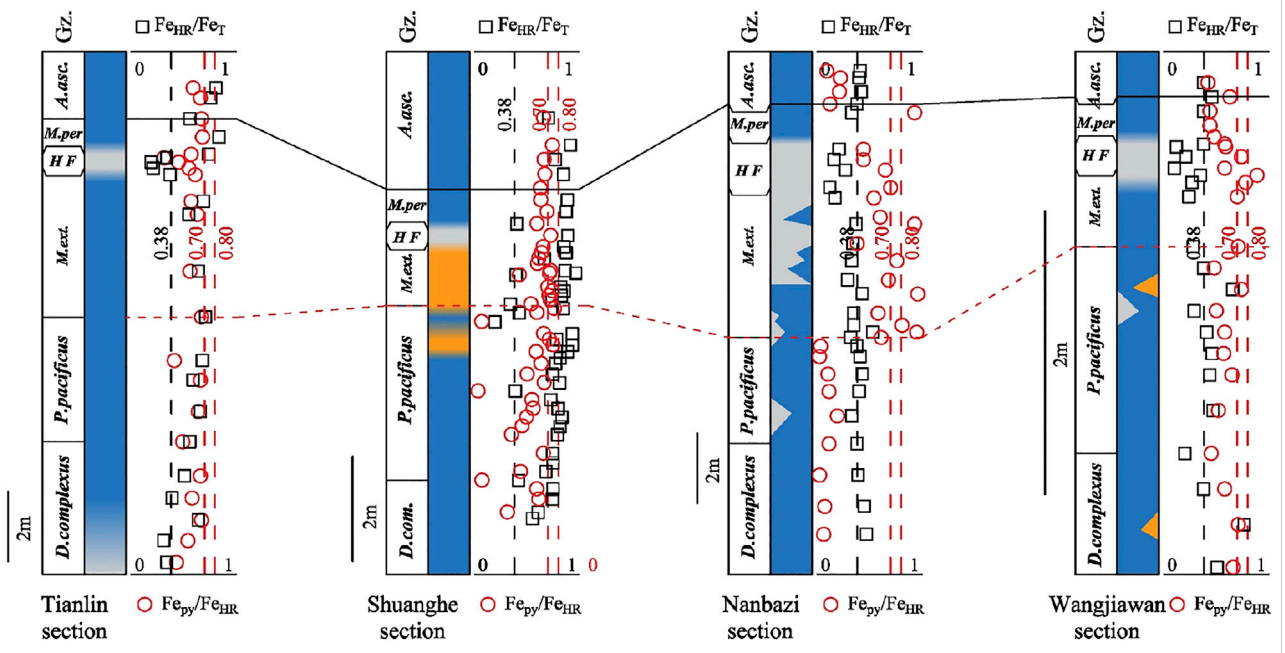

FIGURE 6
Redox condition correlations for the study sections. Data of the Shuanghe section, Nanbazi section, and Wangjiawan section can be found in previous studies (Yan et al., 2009b, 2012; Liu et al., 2016; Li et al., 2017b; Li N et al., 2021; Li Y et al., 2021).

This equation does not take into account the organic carbon loss and related hydrocarbon generation and loss (i.e., via expulsion) during the thermal maturation of OM; the obtained SRI value is thus the minimum OM consumed by the MSR. The greater the value of SRI, the higher the strength of MSR.

It should be noted that the above equations were only applicable to anoxic conditions, without biological disturbance (Ekpo et al., 2012). This is because under anoxic conditions, most of the metabolizable organic carbon can be assumed to be consumed by sulfate reduction, and the generated H_2S is not likely to oxidize and escape from the sediments owing to the protection of large amounts of active iron. Of course, the actual reaction process is more complex, and is controlled by many factors, such as the availability of organic carbon and sulfate. However, the positive exponential relationship between SRI and TOC observed in different modern aquatic environments can confirm the effectiveness of SRI as an index of MSR (Shen et al., 2011). We noted that the value of SRI decreases, and the value of TOC increases with a decrease in the sulfate content from euxinic water to normal seawater and then to fresh water; this represents a decrease in sulfate reduction strength and the preservation of organic carbon.

For the Tianlin section, from the late Katian to Hirnantian and then to early Rhuddanian stages, the value of SRI first decreased and then increased, reaching its minimum value in the GYQ Formation, with an average of 1.27 (Table 1). Owing to limited sample data, no significant correlation was found between SRI and other elements or indicators in the Tianlin section (Table 1). Therefore, we discuss these data in relation to the four other sections within the same basin to understand the impact of SRI on the sediments.

There was a significant power function negative correlation between SRI and TOC ($r = -0.43$, $p < 0.01$, n=117, Figure 7A), indicating that the consumption of active OM increased with increasing MSR intensity. It is worth noting that under different sedimentary environments, TOC values clearly show different trends with a change in SRI (Figure 7A). In euxinic environments (i.e., TS/TOC ≤0.5, SRI ≤1.499) (Berner and Raiswell, 1984; Liu et al., 2021), TOC decreases rapidly with an increase in SRI. Under other environments (SRI >1.499), with the increase in SRI, TOC gradually tends to stabilized (Figure 7A). This indicates that, under anoxic conditions, the availability of active OM was not the main factor limiting MSR in the study area. Additionally, there was a logarithmic negative correlation between SRI and OCAR ($r = -0.22$, $p < 0.05$, $n = 117$, Figure 7B), which further supports the speculation above. For regions with a high TOC content, the value of SRI was low, which may be related to the availability of sulfate in the water column.

The SRI vs. Fe_{py} plot exhibits a significant positive power function relationship ($r = 0.33$, $p < 0.01$, $n = 117$, Figure 7C), indicating that the pyrite in shale was mainly generated by MSR, and that the input of active iron was not the main factor limiting MSR. Additionally, there was a positive logarithmic correlation

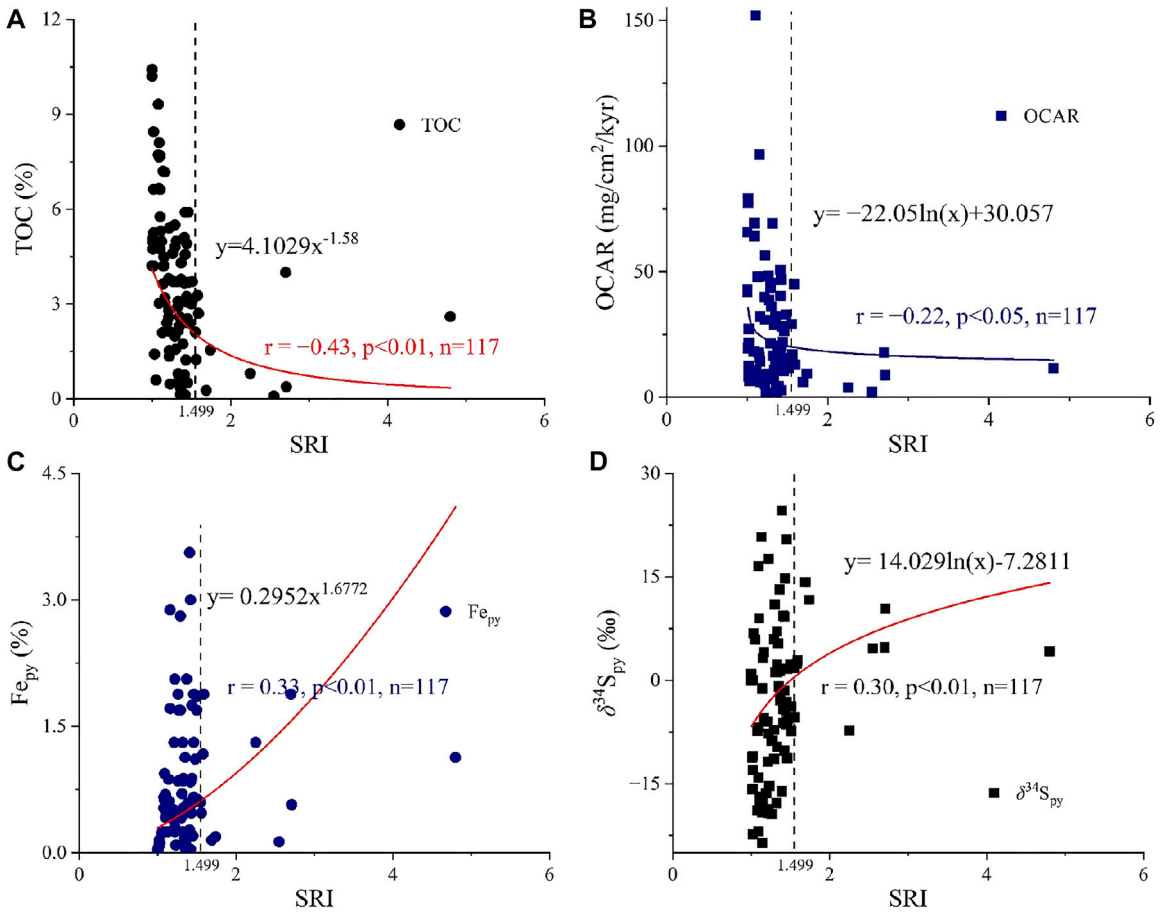

FIGURE 7
Crossplots of SRI vs. **(A)** TOC, **(B)** OCAR, **(C)** Fe_{py} and **(D)** $\delta^{34}S_{py}$.

between SRI and $\delta^{34}S_{py}$ (r = 0.30, $p < 0.01$, n=117, Figure 7D), indicating that MSR was one of the main driving forces for the positive excursion of $\delta^{34}S_{py}$ in the Upper Yangtze Basin. It is noteworthy that this driving force relationship mainly occurs in sulfate limited environments, such as in a closed system and/or porewater (Bradley et al., 2016). In a semi-restricted environment, the Upper Yangtze Basin conforms to this trend. There was no significant relationship between SRI and $\delta^{13}C_{org}$ (data not shown), suggesting that MSR was not the cause of the $\delta^{13}C_{org}$ excursion.

5.3 Impact of volcanic activity on marine sediments

Large-scale volcanic eruptions can cause a series of changes in the atmospheric composition, climate, and biosphere of the earth; most notably, volcanic activity plays an important role in OM enrichment and biological extinction (Ernst and Youbi, 2017). Volcanic activities promote the enrichment of OM via two main pathways. First, emitted volcanic ash and aerosols provide substantial nutrients for marine organisms (e.g., Fe, P, N, Mn, etc.), which improves primary productivity; second, volcanic activities can create an extremely anoxic water environment, which increase the amount of OM (Ge et al., 2019; Wu et al., 2019). Many bentonite rocks were found in the late Katian Stage (*P. pacificus*) and early Rhuddanian Stage (*A. ascensus*) in the Upper Yangtze Basin, confirming the frequent volcanic activity during the O-S transition period (Figure 8). In this study, we used the thickness and layer number of bentonite rocks to discuss their relationship with paleoproductivity and redox conditions.

In the Tianlin section, dense segments of bentonite were mainly concentrated in the early Hirnantian (*Met. extraordinarius*) and early Rhuddanian stages (*A. ascensus*), whereas other segments were loosely distributed (Figure 1C). Evidently, the TOC value of black shale in dense segments was generally higher than that in the loose segments, which indirectly proves that volcanic activity could promote the enrichment of

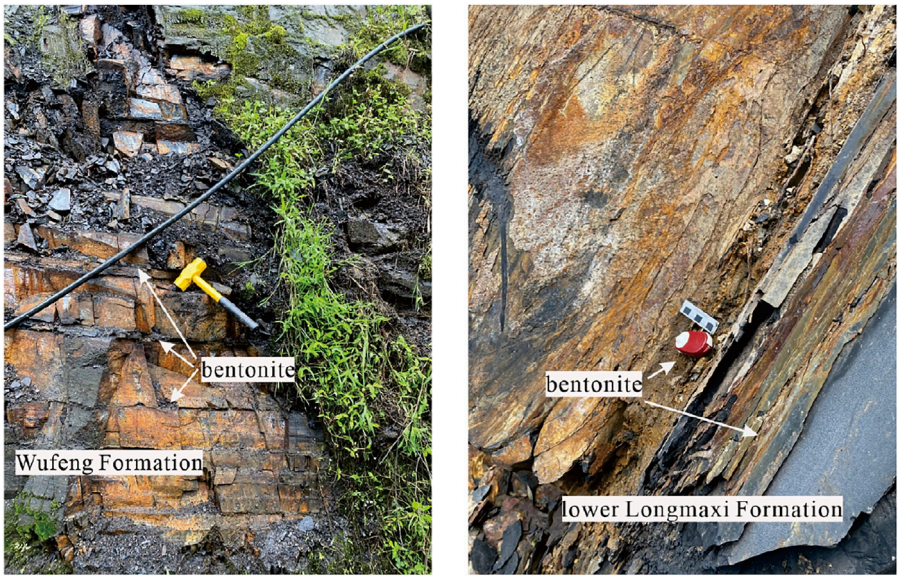

FIGURE 8
Bentonite found in the Wufeng and Longmaxi formations in the Tianlin section.

black OM. Moreover, similar conclusions have been drawn in other sections of the Upper Yangtze Basin (Wu et al., 2018; Li Y et al., 2021). The same corresponding characteristics were also reflected in the relationship of bentonite with OCAR and Fe_{py}/Fe_{HR} (Figure 2), that is, the dense section of bentonite induced an increase marine primary productivity and thereby the lack of oxygen in water columns.

In addition to the thickness of bentonite, the Hg content is one of the most effective proxies indicating the strength of volcanic activity (Sial et al., 2013; Charbonnier et al., 2017; Grasby et al., 2019). In marine systems, Hg can be stored in sediments combined with OM, clay minerals, sulfides and other components (Ravichandran, 2004; Selin, 2009). Organic mercury complexes formed by OM are often the main host of Hg in sediments (Ravichandran, 2004). However, there was no significant correlation between Hg and TOC ($r = 0.27$, $p > 0.1$, n=23, Figure 9A) in the Tianlin section, suggesting that organic mercury was not the main occurrence state of Hg. Additionally, there was no significant correlation between Hg and Al ($r = -0.23$, $p > 0.1$, n=23, Figure 9B); this indicates that clay minerals were also not the main occurrence state of Hg. There was a weak positive correlation between Hg and TS ($r = 0.50$, $p < 0.05$, n=23, Figure 9C) suggested that the occurrence of mercury in sulfide minerals may be a reason for its enrichment. However, there was no significant correlation between Hg and Mo, an indicator that can reflect the redox conditions of water ($r = 0.13$, $p > 0.1$, n = 23, Figure 9D). This indicates that the change in redox conditions did not affect the enrichment of Hg (Algeo and Lyons, 2006; Duan et al., 2016). Alternatively, the rapid formation of sulfide under anoxic conditions did not change the content of Hg. Therefore, we believe that the increased input of atmospheric mercury, associated with volcanic eruptions, may be a valid explanation for Hg enrichment.

Additionally, the location of the dense segments of bentonite and the high Hg content were the same as or close to the negative excursions of $\delta^{13}C_{org}$ and $\delta^{34}S_{py}$, especially in the early Rhuddanian Stage, showing that volcanic activity was the trigger for $\delta^{13}C_{org}$ and $\delta^{34}S_{py}$ disturbances (Figures 1, 2). Li Y et al. (2021) also confirmed this inference using Hg results measured in the same basin.

The CO_2 released by volcanic activities is relatively rich in light carbon isotopes, and these carbon isotope values range from 0‰ to −7.5‰ (average = −5.0‰). Volcanic activities are considered to be the main source of carbon isotope excursions (Hesselbo et al., 2000). Volcanic eruptions release a large amount of CO_2 that is rich in light C isotopes, which can saturate the atmosphere-ocean system. Many carbon sources rich in ^{12}C enter the atmosphere and are absorbed and fixed by marine planktonic algae, one of the main sources of sedimentary OM, through photosynthesis, resulting in negative excursion of carbon isotope in subsequent sediments (Kemp et al., 2005; Wang et al., 2021b; Hu et al., 2022). In addition, it takes a long time for CO_2 from volcanic eruptions to affect the composition of carbon isotopes in seawater, which is consistent with the negative excursion of carbon isotope in the early Rhuddanian Stage, which lasted for nearly 3 Myr. This is in line with the possibility that CO_2 released by volcanic activity may be the main driver of negative

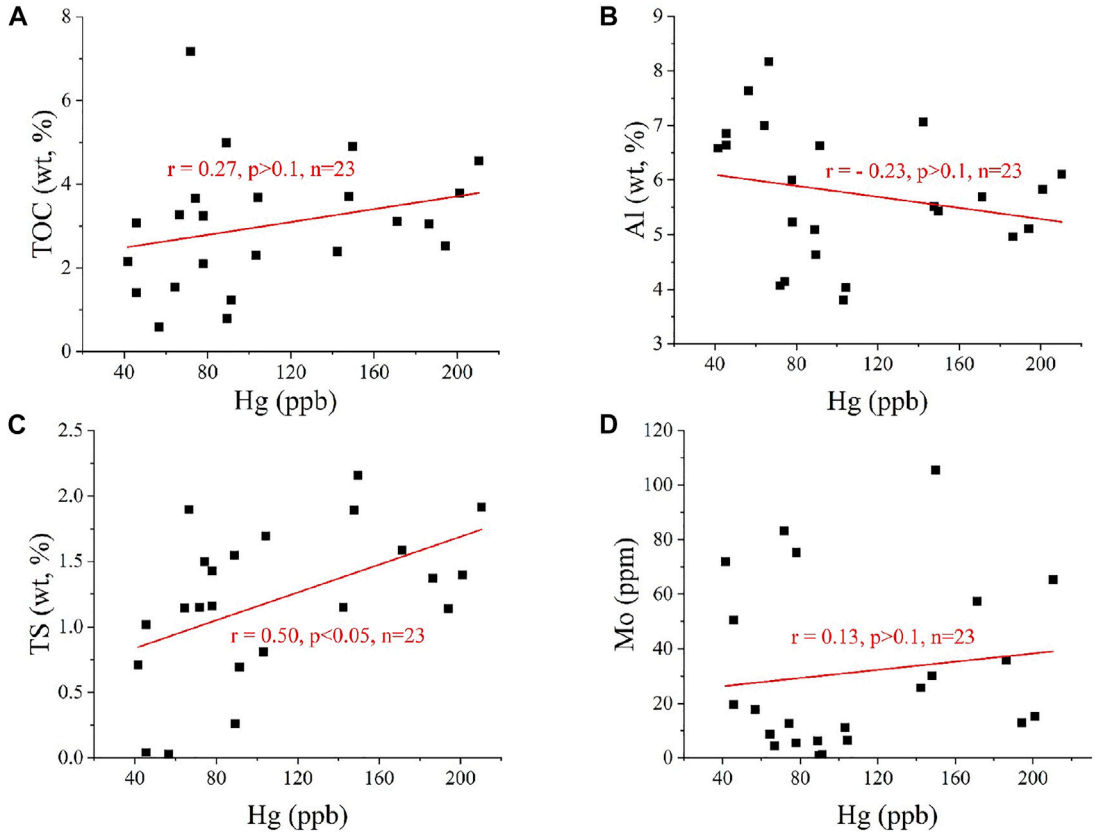

FIGURE 9
Crossplots of Hg with **(A)** TOC, **(B)** Al, **(C)** TS, and **(D)** Mo.

carbon isotope excursion. Science it is a greenhouse gas, an increase in the CO_2 concentration in the atmosphere can induce a prolonged greenhouse effect on earth, translating to increased surface temperatures. This is consistent with glacier melting and sea-level rise events during the Early Silurian.

However, the proportion of sulfate input to the marine environment from volcanic activities is relatively low (<6.0%) (Canfield and Farquhar, 2009), which may cause a significant negative excursion of $\delta^{34}S_{py}$ in a short time. However, there is not certainty that this is the reason for the low value of $\delta^{34}S_{py}$ for a long time. A comprehensive analysis is required to explain the causes of this phenomenon.

5.4 Analysis of $\delta^{34}S_{py}$ variability in hirnantian glaciation

In the MSR process, the lighter ^{32}S is preferentially reduced from sulfate, and the generated sulfide has a lower content $\delta^{34}S$, leaving a residual carbonate reservoir rich in $\delta^{34}S$. Under limited sulfate, and the continuous consumption of MSR, the $\delta^{34}S$ increases gradually, and the difference between the $\delta^{34}S$ value and the residual carbonate reservoir decreases gradually (Canfield, 2001). It is apparent that the value of $\delta^{34}S_{py}$ mainly depends on the sulfur isotope composition of sulfate ($\delta^{34}S_{CAS}$) in the source region and isotope fractionation between sulfate and sulfide ($\Delta^{34}S = \delta^{34}S_{CAS} - \delta^{34}S_{py}$). The magnitude of isotope fractionation ($\Delta^{34}S$) is related to the MSR reaction rate and marine sulfate concentration (Leavitt et al., 2013; Algeo et al., 2015). With sufficiently active OM, an open system featuring a high concentration of sulfate is prone to large isotope fractionation; on the contrary, this increases the reaction rate of MSR, and induces smaller isotope fractionation (Leavitt et al., 2013).

During the O-S transition period, samples from five sections in the Upper Yangtze Basin showed a significant variation in $\delta^{34}S_{py}$, especially during the Hirnantian Stage (Figure 3). Discussions on the causes of this phenomenon mainly focus on whether the marine sulfate concentration changed during this period, that is, whether sulfate availability changed significantly. (Jones and Fike, 2013). analyzed shale samples from Ellis Bay Formation and found that $\delta^{34}S_{CAS}$ did not undergo significant excursions throughout the O-S period. The main reason for the global $\delta^{34}S_{py}$ excursion was the instantaneous decrease in $\Delta^{34}S$ in the microbial sulfur cycle under the influence of abrupt climate change. The transition from anoxic

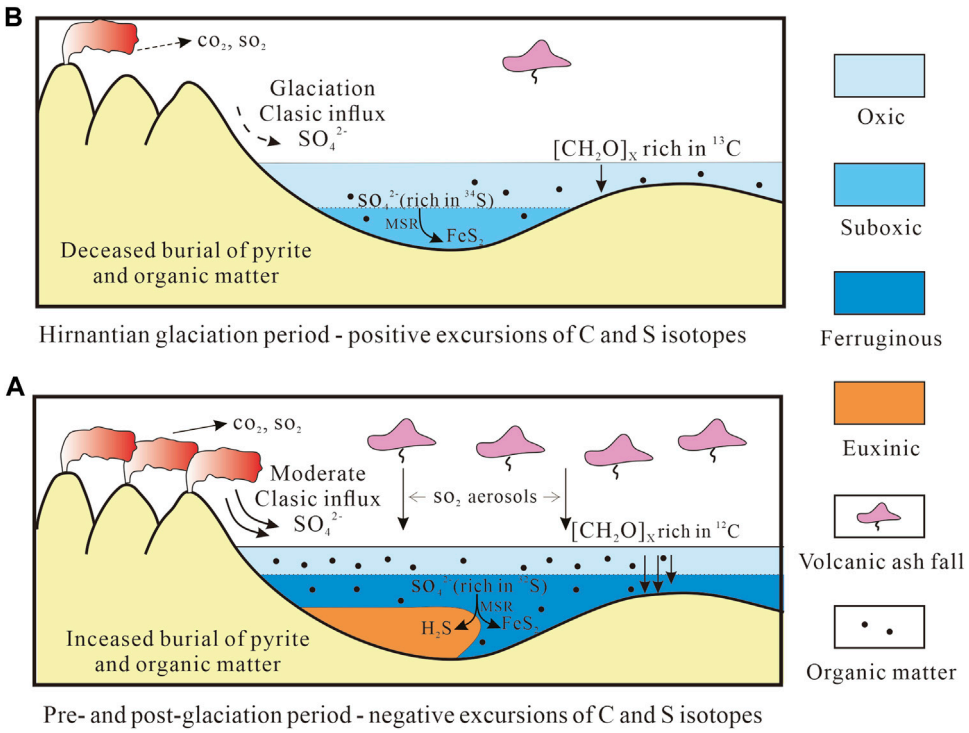

FIGURE 10
Schematic model for the carbon and sulfur cycles in the Upper Yangtze Basin during the O-S period. **(A)** Pre- and post glaciation for the negative excursions of $\delta^{13}C_{org}$ and $\delta^{34}S_{py}$, **(B)** Hirnantian glaciation for the positive excursions of$\delta^{13}C_{org}$ and $\delta^{34}S_{py}$. MSR, microbial sulfate reduction.

conditions to oxic ones caused the chemocline to migrate below the sediment-water interface, where the exchange of sulfate between pore water and overlying water is limited, resulting in a gradual increase in $\delta^{34}S_{py}$ (Yan et al., 2009a; Jones and Fike, 2013). Under these conditions, the framboids generated by MSR should have a large particle size difference, but the pyrite found in the upper Yangtze basin is relatively uniform. It was thus inferred that the framboids were generated in the water column and were the result of synergy (Zou et al., 2018; Li N et al., 2021). Zou et al. (2018), Li N et al. (2021), and Wang et al. (2021a) also found that in the O-S period, the offset of $\delta^{34}S_{py}$ did not appear in a large range like that in a closed system. On the contrary, the positive offset range was small. Therefore, it can be assumed that the reason for the decrease in the $\Delta^{34}S$ value in the Upper Yangtze Basin during the O-S period was a decreased difference between the limited sulfate input and MSR fractionation, rather than the influence of sulfate concentration in pore water.

5.5 Potential causes of $\delta^{13}C_{org}$ and $\delta^{34}S_{py}$ variations

For the C cycle, $\delta^{13}C_{org}$ presented a negative excursion for a long time before the Hirnantian glaciation (i.e., late Katian stage), corresponding to a high TOC content, indicating that a large amount of organic carbon was buried (Figures 2, 10A). The burial of organic carbon removes a large amount of ^{12}C from the marine carbon pool, causing the carbon isotopes in the marine system to become heavier, thereby making the carbon isotopes in the sediments accordingly heavier. At the same time, the burial of a large amount of organic carbon consumes the CO_2 released by volcanic activity in the atmospheric, resulting in a decrease in atmosphere pCO_2 concentrations, leading to a drop in temperature and the cooling of the global climate (Murray, 1994). Additionally, sulfur species (i.e., SO_2, H_2S, and COS) emitted by volcanic activities also control climate change. These sulfur species can be rapidly oxidized into sulfate in the troposphere and washed out of the atmosphere (McCormick et al., 1995; Mather, 2015; Hu et al., 2020). In the stratosphere, sulfate will backscatter the short-wave solar radiation in the form of aerosols, and absorb the long-wave radiation, making the temperature on the Earth's surface decreased, resulting in global cooling (McCormick et al., 1995; Mather, 2015). This variability was similar to those of climate and $\delta^{13}C_{org}$ changes in the Hirnantian period, indicating that carbon burial was the direct reason for the positive excursion of $\delta^{13}C_{org}$ (Figure 10B). This, of course, the composition of $\delta^{13}C_{org}$ was not only affected by

the atmospheric pCO_2 concentrations, but also affected by the secondary productivity, terrestrial OM, and marine dissolved organic carbon (Bekker et al., 2008; Jiang et al., 2010; Jiang et al., 2012). Recent studies on multiple proxies of biomarkers showed that the planktonic algae was the main source of OM during this period (Zhang et al., 2020; Wang et al., 2021b). Meanwhile, the values of ∑steranes/∑hopanes and steranes C_{27}/C_{29} were used to exclude the contribution of bacteria and terrestrial plants to sedimentary OM (Zhang et al., 2020). Therefore, the convincing explanation for the excursion of $\delta^{13}C$ during this period is that planktonic algae can gradually consume CO_2 in the water column through photosynthesis, which makes the $\delta^{13}C$ is gradually enriched in the newly generated sedimentary OM.

During the post-glaciation period, with the warming of the climate and the recovery of volcanic activity, the concentration of CO_2 in the atmosphere increased, and the ^{12}C input into the marine environment rapidly increased, triggering the negative excursion of $^{13}C_{org}$ (Figure 10A). Additionally, TOC and $\delta^{13}C_{org}$ showed no significant correlation, and carbonate sedimentary facies were not found in the Upper Yangtze Basin, indicating that carbonate weathering was not the reason for the positive deviation in $\delta^{13}C_{org}$ (Chen et al., 2004).

For the S cycle, during the pre-glaciation period, hot and humid climatic conditions and strong weathering increased the input of terrestrial sulfates, coupled with frequent volcanic activity, this resulted in the continuous input of ^{32}S-rich sulfates to produce ^{34}S-poor sulfides under the MSR (Figure 10A). During the Hirnantian glaciation period, rivers were frozen, sea levels fell, and the terrestrial input of sulfate was blocked, further reinforcing the limitations experienced by the basin. At this time, different degrees of anoxic conditions occurred in water columns, at different locations, resulting in different level of sulfur isotope fractionation. Nevertheless, the generated sulfide gradually enriched ^{34}S and reached its maximum in the GYQ Formation (Figure 10B).

During the post-glaciation period, as the temperature rose, the ice sheet melted, the sea level rose, the volcanic activity was restored, weathering was enhanced, and rivers recovered. Overall, this resulted in inputs of sulfate to rapidly increase within the basin, and the sulfide rich in ^{32}S deposited under the action of MSR throughout the Rhuddanian Stage (Figure 10A).

6 Conclusion

A high-resolution analysis of $\delta^{13}C_{org}$, and $\delta^{34}S_{py}$ was conducted for the Tianlin section, and combined with data for four previously published sections, our study provides new insights into the isotopic disturbances and factors underlying the Hirnantian glaciation period in the Upper Yangtze Basin. Under semi-restricted conditions, the influence of warm climatic conditions and terrigenous clastic inputs caused by strong weathering caused the Upper Yangtze Basin to have a high primary productivity. This state was maintained until the early Hirnantian Stage, which promoted carbon burial and led to positive excursions of $\delta^{13}C_{org}$. During post-glaciation, the temperature and primary productivity gradually recovered under the influence of volcanic activity, resulting in negative excursions of $\delta^{13}C_{org}$. The excursion of $\delta^{34}S_{py}$ can be explained through the lens of several factors. During pre- and post-glaciation, because of an increase in terrestrial sulfate input and the influence of volcanic activity, the sulfides produced by MSR had lower $\delta^{34}S_{py}$. Additionally, during Hirnantian glaciation, the availability of sulfate decreased, and under the action of MSR, sulfate in the water gradually enriched $\delta^{34}S$, thereby producing sulfides with high $\delta^{34}S$ levels. The low values of $\delta^{13}C_{org}$ and $\delta^{34}S_{py}$ in pre- and post-glaciation sections coincided with the strengthened volcanic activity, indicating that volcanic activity was a major mechanism for the negative excursion of $\delta^{13}C_{org}$ and $\delta^{34}S_{py}$. This study emphasizes the complex influence of volcanic activity and MSR on carbon and sulfur cycle disturbances and environmental changes in semi-restricted basins.

Data availability statement

The original contributions presented in the study are included in the article/supplementary material, further inquiries can be directed to the corresponding authors.

Author contributions

Investigation, ZD and ZW; Methodology, WZ and FZ; review and editing YD and XF; data curation, ZW and YZ; writing original draft, ZD; funding acquisition, CW.

Funding

This study was funded by the National Natural Science Foundation of China (No. 41772129).

Conflict of interest

Author FZ is employed by Xuzhou Datun Engineering Consulting Co., Ltd.

The remaining authors declare that the research was conducted in the absence of any commercial or financial relationships that could be construed as a potential conflict of interest.

Publisher's note

References

Algeo, T. J., Luo, G. M., Song, H. Y., Lyons, T. W., and Canfield, D. E. (2015). Reconstruction of secular variation in seawater sulfate concentrations. *Biogeosciences* 12, 2131–2151. doi:10.5194/bg-12-2131-2015

Algeo, T. J., and Lyons, T. W. (2006). Mo-total organic carbon covariation in modern anoxic marine environments: Implications for analysis of paleoredox and paleohydrographic conditions. *Paleoceanography* 21. doi:10.1029/2004PA001112

Algeo, T. J., and Rowe, H. (2012). Paleoceanographic applications of trace-metal concentration data. *Chem. Geol.* 324, 6–18. doi:10.1016/j.chemgeo.2011.09.002

Algeo, T. J., and Tribovillard, N. (2009). Environmental analysis of paleoceanographic systems based on molybdenum–uranium covariation. *Chem. Geol.* 268, 211–225. doi:10.1016/j.chemgeo.2009.09.001

Bekker, A., Holmden, C., Beukes, N. J., Kenig, F., Eglingtone, B., and Patterson, W. (2008). Fractionation between inorganic and organic carbon during the Lomagundi (2.22-2.1 Ga) carbon isotope excursion. *Earth Planet. Sci. Lett.* 271, 278–291. doi:10.1016/j.epsl.2008.04.021

Berner, R. A., and Raiswell, R. (1984). C/S method for distinguishing freshwater from marine sedimentary rocks. *Geol.* 12, 365–368. doi:10.1130/0091-7613(1984)12<365:CMFDFF>2.0.CO;2

Bradley, A. S., Leavitt, W. D., Schmidt, M., Knoll, A. H., Girguis, P. R., and Johnston, D. T. (2016). Patterns of sulfur isotope fractionation during microbial sulfate reduction. *Geobiology* 14, 91–101. doi:10.1111/gbi.12149

Brenchley, P. J., Carden, G. A., Hints, L., Kaljo, D., Marshall, J. D., Martma, T., et al. (2003). High-resolution stable isotope stratigraphy of Upper Ordovician sequences: Constraints on the timing of bioevents and environmental changes associated with mass extinction and glaciation. *Geol. Soc. Am. Bull.* 115, 89–104. doi:10.1130/0016-7606(2003)115<0089:HRSISO>2.0.CO;2

Canfield, D. E. (2001). Biogeochemistry of sulfur isotopes. *Rev. Mineral. Geochem.* 43, 607–636. doi:10.2138/gsrmg.43.1.607

Canfield, D. E., and Farquhar, J. (2009). Animal evolution, bioturbation, and the sulfate concentration of the oceans. *Proc. Natl. Acad. Sci. U. S. A.* 106, 8123–8127. doi:10.1073/pnas.0902037106

Charbonnier, G., Morales, C., Duchamp-Alphonse, S., Westermann, S., Adatte, T., and Follmi, K. B. (2017). Mercury enrichment indicates volcanic triggering of Valanginian environmental change. *Sci. Rep.* 7, 40808. doi:10.1038/srep40808

Chen, X., Rong, J., Li, Y., and Boucot, A. J. (2004). Facies patterns and geography of the yangtze region, south China, through the ordovician and silurian transition. *Palaeogeogr. Palaeoclimatol. Palaeoecol.* 204, 353–372. doi:10.1016/S0031-0182(03)00736-3

Chen, X., Rong, J., Mitchell, C. E., Happer, D. A. T., Fan, J., Renbin, Z., et al. (2000). Late Ordovician to earliest Silurian graptolite and brachiopod biozonation from the Yangtze region, South China, with a global correlation. *Geol. Mag.* 137, 623–650. doi:10.1017/S0016756800004702

Cooper, R. A., Rigby, S., Loydell, D. K., and Bates, D. E. B. (2012). Palaeoecology of the graptoloidea. *Earth. Sci. Rev.* 112, 23–41. doi:10.1016/j.earscirev.2012.01.001

Dong, Z., Wang, Z., Zhang, W., Cheng, S., Fu, X., and Wang, C. (2022). Distribution characteristics and genesis of marine anoxic conditions in the southwest of the upper yangtze basin during the late ordovician–early silurian, south China. *Front. Earth Sci. (Lausanne).* 10. doi:10.3389/feart.2022.934488

Duan, Y., Han, D. S., Batchelor, B., and Abdel-Wahab, A. (2016). Synthesis, characterization, and application of pyrite for removal of mercury. *Colloids Surfaces A Physicochem. Eng. Aspects* 490, 326–335. doi:10.1016/j.colsurfa.2015.11.057

Ekpo, B. O., Ibok, U. J., Essien, N., and Wehner, H. (2012). Geochemistry and organic petrography of Cretaceous sediments of the Calabar Flank, southeastern, Nigeria. *Mar. Pet. Geol.* 35, 252–268. doi:10.1016/j.marpetgeo.2012.03.010

Elrick, M., Reardon, D., Labor, W., Martin, J., Desrochers, A., and Pope, M. (2013). Orbital-scale climate change and glacioeustasy during the early Late Ordovician (pre-Hirnantian) determined from δ18O values in marine apatite. *Geology* 41, 775–778. doi:10.1130/G34363.1

Ernst, R. E., and Youbi, N. (2017). How Large Igneous Provinces affect global climate, sometimes cause mass extinctions, and represent natural markers in the geological record. *Palaeogeogr. Palaeoclimatol. Palaeoecol.* 478, 30–52. doi:10.1016/j.palaeo.2017.03.014

Fan, J., Peng, P., and Melchin, M. J. (2009). Carbon isotopes and event stratigraphy near the Ordovician-Silurian boundary, Yichang, South China. *Palaeogeogr. Palaeoclimatol. Palaeoecol.* 276, 160–169. doi:10.1016/j.palaeo.2009.03.007

Finnegan, S., Bergmann, K., Eiler, J. M., Jones, D. S., Fike, D. A., Eisenman, I., et al. (2011). The magnitude and duration of late Ordovician-Early silurian glaciation. *Science* 331, 903–906. doi:10.1126/science.1200803

Ge, X., Mou, C., Yu, Q., Liu, W., Men, X., and He, J. (2019). The geochemistry of the sedimentary rocks from the Huadi No. 1 well in the Wufeng-Longmaxi formations (Upper Ordovician-Lower Silurian), South China, with implications for paleoweathering, provenance, tectonic setting and paleoclimate. *Mar. Pet. Geol.* 103, 646–660. doi:10.1016/j.marpetgeo.2018.12.040

Gibbs, M. T., Barron, E. J., and Kump, L. R. (1997). An atmospheric pCO(2) threshold for glaciation in the Late Ordovician. *Geol.* 25, 447–450. doi:10.1130/0091-7613(1997)025<0447:AAPCTF>2.3.CO;2

Gill, B. C., Lyons, T. W., Young, S. A., Kump, L. R., Knoll, A. H., and Saltzman, M. R. (2011). Geochemical evidence for widespread euxinia in the Later Cambrian ocean. *Nature* 469, 80–83. doi:10.1038/nature09700

Gomes, M. L., and Hurtgen, M. T. (2015). Sulfur isotope fractionation in modern euxinic systems: Implications for paleoenvironmental reconstructions of paired sulfate–sulfide isotope records. *Geochim. Cosmochim. Acta* 157, 39–55. doi:10.1016/j.gca.2015.02.031

Gorjan, P., Kaiho, K., Fike, D. A., and Xu, C. (2012). Carbon- and sulfur-isotope geochemistry of the hirnantian (late ordovician) wangjiawan (riverside) section, south China: Global correlation and environmental event interpretation. *Palaeogeogr. Palaeoclimatol. Palaeoecol.* 337, 14–22. doi:10.1016/j.palaeo.2012.03.021

Grasby, S. E., Them, T. R. I., Chen, Z., Yin, R., and Ardakani, O. H. (2019). Mercury as a proxy for volcanic emissions in the geologic record. *Earth. Sci. Rev.* 196, 102880. doi:10.1016/j.earscirev.2019.102880

Hambrey, M. J. (1985). The late Ordovician-early Silurian glacial period. *Palaeogeogr. Palaeocl.*

Hammarlund, E. U., Dahl, T. W., Harper, D. A. T., Bond, D. P. G., Nielsen, A. T., Bjerrum, C. J., et al. (2012). A sulfidic driver for the end-Ordovician mass extinction. *Earth Planet. Sci. Lett.* 331-332, 128–139. doi:10.1016/j.epsl.2012.02.024

Herrmann, A. D., Haupt, B. J., Patzkowsky, M. E., Seidov, D., and Slingerland, R. L. (2004). Response of Late Ordovician paleoceanography to changes in sea level, continental drift, and atmospheric pCO(2): Potential causes for long-term cooling and glaciation. *Palaeogeogr. Palaeoclimatol. Palaeoecol.* 210, 385–401. doi:10.1016/j.palaeo.2004.02.034

Hesselbo, S. P., Grocke, D. R., Jenkyns, H. C., Bjerrum, C. J., Farrimond, P., Morgans Bell, H. S., et al. (2000). Massive dissociation of gas hydrate during a Jurassic oceanic anoxic event. *Nature* 406, 392–395. doi:10.1038/35019044

Hu, D., Li, M., Zhang, X., Turchyn, A. V., Gong, Y., and Shen, Y. (2020). Large mass-independent sulphur isotope anomalies link stratospheric volcanism to the Late Ordovician mass extinction. *Nat. Commun.* 11, 2297. doi:10.1038/s41467-020-16228-2

Hu, F., Meng, Q., and Liu, Z. (2022). Petrological and geochemical characteristics of coal and oil shale of Paleogene Lijiaya Formation in Huangxian Basin, Eastern China: Implication for evolution of symbiotic formation mechanism. *Geomech. Geophys. Geo. Energy. Ge. Resour.* 8, 123. doi:10.1007/s40948-022-00428-9

Hurtgen, M. T. (2012). The marine sulfur cycle, revisited. *Science* 337, 305–306. doi:10.1126/science.1225461

Jiang, G., Wang, X., Shi, X., Xiao, S., Zhang, S., and Dong, J. (2012). The origin of decoupled carbonate and organic carbon isotope signatures in the early Cambrian (ca. 542-520 Ma) Yangtze platform. *Earth Planet. Sci. Lett.* 317, 96–110. doi:10.1016/j.epsl.2011.11.018

Jiang, G., Wang, X., Shi, X., Zhan, S., Xiao, S., and Dong, J. (2010). Organic carbon isotope constraints on the dissolved organic carbon (DOC) reservoir at the

Cryogenian-Ediacaran transition. *Earth Planet. Sci. Lett.* 299, 159–168. doi:10.1016/j.epsl.2010.08.031

Johnston, D. T., Wing, B. A., Farquhar, J., Kaufman, A. J., Strauss, H., Lyons, T. W., et al. (2005). Active microbial sulfur disproportionation in the Mesoproterozoic. *Science* 310, 1477–1479. doi:10.1126/science.1117824

Jones, D. S., and Fike, D. A. (2013). Dynamic sulfur and carbon cycling through the end-Ordovician extinction revealed by paired sulfate–pyrite δ34S. *Earth Planet. Sci. Lett.* 363, 144–155. doi:10.1016/j.epsl.2012.12.015

Jones, D. S., Fike, D. A., Finnegan, S., Fischer, W. W., Schrag, D. P., and McCay, D. (2011). Terminal Ordovician carbon isotope stratigraphy and glacioeustatic sea-level change across Anticosti Island (Quebec, Canada). *Geol. Soc. Am. Bull.* 123, 1645–1664. doi:10.1130/B30323.1

Kemp, D. B., Coe, A. L., Cohen, A. S., and Schwark, L. (2005). Astronomical pacing of methane release in the Early Jurassic period. *Nature* 437, 396–399. doi:10.1038/nature04037

Kiipli, T., Kiipli, E., and Kaljo, D. (2010). Silurian sea level variations estimated using SiO2/Al2O3 and K2O/Al2O3 ratios in the Priekule drill core section, Latvia. *B Soc. Paleontol. Ital.* 49, 55–63.

Kump, L. R., and Arthur, M. A. (1999). Interpreting carbon-isotope excursions: Carbonates and organic matter. *Chem. Geol.* 161, 181–198. doi:10.1016/S0009-2541(99)00086-8

Lallier-Verges, E., Bertrand, P., and Desprairies, A. (1993). Organic matter composition and sulfate reduction intensity in Oman margin sediments. *Mar. Geol.* 112, 57–69. doi:10.1016/0025-3227(93)90161-n

Leavitt, W. D., Halevy, I., Bradley, A. S., and Johnston, D. T. (2013). Influence of sulfate reduction rates on the Phanerozoic sulfur isotope record. *Proc. Natl. Acad. Sci. U. S. A.* 110, 11244–11249. doi:10.1073/pnas.1218874110

Li, C., Planavsky, N. J., Love, G. D., Reinhard, C. T., Hardisty, D., Feng, L., et al. (2015). Marine redox conditions in the middle Proterozoic ocean and isotopic constraints on authigenic carbonate formation: Insights from the Chuanlinggou Formation, Yanshan Basin, North China. *Geochim. Cosmochim. Acta* 150, 90–105. doi:10.1016/j.gca.2014.12.005

Li, N., Li, C., Algeo, T. J., Cheng, M., Jin, C., Zhu, G., et al. (2021). Redox changes in the outer Yangtze Sea (South China) through the Hirnantian Glaciation and their implications for the end-Ordovician biocrisis. *Earth. Sci. Rev.* 212, 103443. doi:10.1016/j.earscirev.2020.103443

Li, N., Li, C., Fan, J., Algeo, T. J., Yan, D., Zhu, G., et al. (2019). Sulfate-controlled marine euxinia in the semi-restricted inner Yangtze Sea (South China) during the Ordovician-Silurian transition. *Palaeogeogr. Palaeoclimatol. Palaeoecol.* 534, 109281. doi:10.1016/j.palaeo.2019.109281

Li, Y., Schieber, J., Fan, T., Li, Z., and Zhang, J. (2017a). Regional depositional changes and their controls on carbon and sulfur cycling across the Ordovician-Silurian boundary, northwestern Guizhou, South China. *Palaeogeogr. Palaeoclimatol. Palaeoecol.* 485, 816–832. doi:10.1016/j.palaeo.2017.07.039

Li, Y., Zhang, T., Ellis, G. S., and Shao, D. (2017b). Depositional environment and organic matter accumulation of upper ordovician-lower silurian marine shale in the upper yangtze platform, south China. *Palaeogeogr. Palaeoclimatol. Palaeoecol.* 466, 252–264. doi:10.1016/j.palaeo.2016.11.037

Li, Y., Zhang, T., Shen, B., Li, Z., Shao, D., and Lash, G. G. (2021). Carbon and sulfur isotope variations through the upper ordovician and lower silurian of south China linked to volcanism. *Palaeogeogr. Palaeoclimatol. Palaeoecol.* 567, 110285. doi:10.1016/j.palaeo.2021.110285

Liu, Q., Li, P., Jin, Z., Liang, X., Zhu, D., Wu, X., et al. (2021). Preservation of organic matter in shale linked to bacterial sulfate reduction (BSR) and volcanic activity under marine and lacustrine depositional environments. *Mar. Pet. Geol.* 127, 104950. doi:10.1016/j.marpetgeo.2021.104950

Liu, Y., Li, C., Algeo, T. J., Fan, J., and Peng, P. (2016). Global and regional controls on marine redox changes across the Ordovician-Silurian boundary in South China. *Palaeogeogr. Palaeoclimatol. Palaeoecol.* 463, 180–191. doi:10.1016/j.palaeo.2016.10.006

Lv, Y., Liu, S., Wu, H., Sun, Z., Li, C., and Fan, J. (2022). Enhanced organic carbon burial intensified the end-Ordovician glaciation. *Geochem. Perspect. Lett.* 21, 13–17. doi:10.7185/geochemlet.2210

Mather, T. A. (2015). Volcanoes and the environment: Lessons for understanding Earth's past and future from studies of present-day volcanic emissions. *J. Volcanol. Geotherm. Res.* 304, 160–179. doi:10.1016/j.jvolgeores.2015.08.016

McCormick, M. P., Thomason, L. W., and Trepte, C. R. (1995). Atmospheric effects of the Mt Pinatubo eruption. *Nature* 373, 399–404. doi:10.1038/373399a0

Munnecke, A., Calner, M., Harper, D. A. T., and Servais, T. (2010). Ordovician and Silurian sea-water chemistry, sea level, and climate; A synopsis. *Palaeogeogr. Palaeoclimatol. Palaeoecol.* 296, 389–413. doi:10.1016/j.palaeo.2010.08.001

Murray, R. W. (1994). Chemical criteria to identify the depositional environment of chert: General principles and applications. *Sediment. Geol.* 90, 213–232. doi:10.1016/0037-0738(94)90039-6

Pope, M. C., and Steffen, J. B. (2003). Widespread, prolonged late middle to late ordovician upwelling in north America: A proxy record of glaciation? *Geol.* 31, 63–66. doi:10.1130/0091-7613(2003)031<0063:WPLMTL>2.0.CO;2

Poulton, S. W., and Canfield, D. E. (2011). Ferruginous conditions; A dominant feature of the ocean through Earth's history. *Elem. (Quebec)* 7, 107–112. doi:10.2113/gselements.7.2.107

Qing, H. R., and Veizer, J. (1994). Oxygen and carbon isotopic composition of ordovician brachiopods - implications for coeval seawater. *Geochim. Cosmochim. Acta* 58, 4429–4442. doi:10.1016/0016-7037(94)90345-X

Raiswell, R., and Canfield, D. E. (2012). The iron biogeochemical cycle past and present. *Geochem. Perspect.* 1. 220, doi:10.7185/geochempersp.1.1

Ravichandran, M. (2004). Interactions between mercury and dissolved organic matter - a review. *Chemosphere* 55, 319–331. doi:10.1016/j.chemosphere.2003.11.011

Rowe, H. D., Loucks, R. G., Ruppel, S. C., and Rimmer, S. M. (2008). Mississippian barnett formation, fort worth basin, Texas: Bulk geochemical inferences and Mo-TOC constraints on the severity of hydrographic restriction. *Chem. Geol.* 257, 16–25. doi:10.1016/j.chemgeo.2008.08.006

Schoepfer, S. D., Shen, J., Wei, H., Tyson, R. V., Ingall, E., and Algeo, T. J. (2015). Total organic carbon, organic phosphorus, and biogenic barium fluxes as proxies for paleomarine productivity. *Earth. Sci. Rev.* 149, 23–52. doi:10.1016/j.earscirev.2014.08.017

Selin, N. E. (2009). Global biogeochemical cycling of mercury: A review. *Annu. Rev. Environ. Resour.* 34, 43–63. doi:10.1146/annurev.environ.051308.084314

Sheehan, P. M. (2001). The Late Ordovician mass extinction. *Annu. Rev. Earth Planet. Sci.* 29, 331–364. doi:10.1146/annurev.earth.29.1.331

Shen, J., Schoepfer, S. D., Feng, Q., Zhou, L., Yu, J., Song, H., et al. (2015). Marine productivity changes during the end-Permian crisis and Early Triassic recovery. *Earth-Science Rev.* 149, 136–162. doi:10.1016/j.earscirev.2014.11.002

Shen, Y., Farquhar, J., Zhang, H., Masterson, A., Zhang, T., and Wing, B. A. (2011). Multiple S-isotopic evidence for episodic shoaling of anoxic water during Late Permian mass extinction. *Nat. Commun.* 2, 210. doi:10.1038/ncomms1217

Sial, A. N., Lacerda, L. D., Ferreira, V. P., Frei, R., Marquillas, R. A., Barbosa, J., et al. (2013). Mercury as a proxy for volcanic activity during extreme environmental turnover: The Cretaceous-Paleogene transition. *Palaeogeogr. Palaeoclimatol. Palaeoecol.* 387, 153–164. doi:10.1016/j.palaeo.2013.07.019

Sutcliffe, O. E., Dowdeswell, J. A., Whittington, R. J., Theron, J. N., and Craig, J. (2000). Calibrating the Late Ordovician glaciation and mass extinction by the eccentricity cycles of Earth's orbit. *Geology* 28, 967–970. doi:10.1130/0091-7613(2000)028<0967:CTLOGA>2.3.CO;2

Taylor, S. R., and McClcnnan, S. M. (1985). *The continental crust: Its composition and evolution*. Blackwell Scientific Publications.

Tribovillard, N., Algeo, T. J., Baudin, F., and Riboulleau, A. (2012). Analysis of marine environmental conditions based on molybdenum-uranium covariation-Applications to Mesozoic paleoceanography. *Chem. Geol.* 324, 46–58. doi:10.1016/j.chemgeo.2011.09.009

Trotter, J. A., Williams, I. S., Barnes, C. R., Lecuyer, C., and Nicoll, R. S. (2008). Did cooling oceans trigger ordovician biodiversification? Evidence from conodont thermometry. *Science* 321, 550–554. doi:10.1126/science.1155814

Tumer, B. R., Makhlouf, I. M., and Armstrong, H. A. (2005). Late Ordovician (Ashgillian) glacial deposits in southern Jordan. *Sediment. Geol.* 181, 73–91. doi:10.1016/j.sedgeo.2005.08.004

Veto, I., Hetenyi, M., Demeny, A., and Hertelendi, E. (1994). Hydrogen index as reflecting intensity of sulphidic diagenesis in non-bioturbated, shaly sediments. *Org. Geochem.* 22, 299–310. doi:10.1016/0146-6380(94)90176-7

Wang, C., Dong, Z., Fu, X., Chen, Q., Liu, X., Tang, M., et al. (2021a). Spatiotemporal evolution and genesis of the late Ordovician-Early silurian marine euxinia in northeastern upper yangtze basin, south China. *Front. Earth Sci. (Lausanne).* 9. doi:10.3389/feart.2021.788349

Wang, C., Dong, Z., Fu, X., Hu, X., and Li, Z. (2021b). Origin and paleoenvironment of organic matter in the Wufeng–Longmaxi shales in the northeastern Sichuan basin. *Energy Explor. Exploitation* 39, 134–155. doi:10.1177/0144598720978007

Wu, L., Lu, Y., Jiang, S., Liu, X., and He, G. (2018). Effects of volcanic activities in ordovician wufeng-silurian Longmaxi period on organic-rich shale in the upper yangtze area, south China. *Petroleum Explor. Dev.* 45, 862–872. doi:10.1016/S1876-3804(18)30089-2

Wu, L., Lu, Y., Jiang, S., Liu, X., Liu, Z., and Lu, Y. (2019). Relationship between the origin of organic-rich shale and geological events of the Upper Ordovician-Lower Silurian in the Upper Yangtze area. *Mar. Pet. Geol.* 102, 74–85. doi:10.1016/j.marpetgeo.2018.11.017

Xi, Z., Tang, S., Lash, G. G., Zhang, B., and Lin, D. (2021). Geochemical characteristics of organic carbon and pyrite sulfur in Ordovician-Silurian transition shales in the Yangtze Platform, South China: Implications for the depositional environment. *Palaeogeogr. Palaeoclimatol. Palaeoecol.* 563, 110173. doi:10.1016/j.palaeo.2020.110173

Yan, D., Chen, D., Wang, Q., and Wang, J. (2009b). Geochemical changes across the ordovician-silurian transition on the yangtze platform, south China. *Sci. China Ser. D-Earth. Sci.* 52, 38–54. doi:10.1007/s11430-008-0143-z

Yan, D., Chen, D., Wang, Q., and Wang, J. (2012). Predominance of stratified anoxic Yangtze Sea interrupted by short-term oxygenation during the Ordo-Silurian transition. *Chem. Geol.* 291, 69–78. doi:10.1016/j.chemgeo.2011.09.015

Yan, D., Chen, D., Wang, Q., Wang, J., and Wang, Z. (2009a). Carbon and sulfur isotopic anomalies across the ordovician-silurian boundary on the yangtze platform, south China. *Palaeogeogr. Palaeoclimatol. Palaeoecol.* 274, 32–39. doi:10.1016/j.palaeo.2008.12.016

Yang, S., Hu, W., and Wang, X. (2021). Mechanism and implications of upwelling from the late ordovician to early silurian in the yangtze region, south China. *Chem. Geol.* 565, 120074. doi:10.1016/j.chemgeo.2021.120074

Zhang, P., Meng, Q., Liu, Z., and Hu, F. (2021a). Mineralogy and geochemistry of the lower cretaceous jiufotang formation, beipiao basin, NE China: Implications for weathering, provenance, and tectonic setting. *ACS Earth Space Chem.* 5, 1288–1305. doi:10.1021/acsearthspacechem.0c00216

Zhang, P., Meng, Q., Misch, D., Sachsenhofer, R. F., Liu, Z., Hu, F., et al. (2021b). Oil shale potential of the lower cretaceous jiufotang formation, beipiao basin, Northeast China. *Int. J. Coal Geol.* 236, 103640. doi:10.1016/j.coal.2020.103640

Zhang, T., Shen, Y., Zhan, R., Shen, S., and Chen, X. (2009). Large perturbations of the carbon and sulfur cycle associated with the Late Ordovician mass extinction in South China. *Geology* 37, 299–302. doi:10.1130/G25477A.1

Zhang, Y., He, Z., Lu, S., Jiang, S., Xiao, D., Long, S., et al. (2020). Characteristics of microorganisms and origin of organic matter in Wufeng Formation and Longmaxi formation in sichuan basin, south China. *Mar. Pet. Geol.* 111, 363–374. doi:10.1016/j.marpetgeo.2019.06.054

Zhou, L., Algeo, T. J., Shen, J., Hu, Z., Gong, H., Xie, S., et al. (2015). Changes in marine productivity and redox conditions during the Late Ordovician Hirnantian glaciation. *Palaeogeogr. Palaeoclimatol. Palaeoecol.* 420, 223–234. doi:10.1016/j.palaeo.2014.12.012

Zou, C., Qiu, Z., Wei, H., Dong, D., and Lu, B. (2018). Euxinia caused the Late Ordovician extinction: Evidence from pyrite morphology and pyritic sulfur isotopic composition in the Yangtze area, South China. *Palaeogeogr. Palaeoclimatol. Palaeoecol.* 511, 1–11. doi:10.1016/j.palaeo.2017.11.033